Aligned Magnetic field and Heat transfer Analysis of radiative Casson Hybrid Nanofluid flow through a porous medium over an inclined plate

Tanuja T N[1,a], Kavitha L[1,b], S V K Varma[1,c], V C C Raju[2] and T G Motsumi[3]

[1]Department of Mathematics, School of Applied Sciences, REVA University, Bengaluru, Karnataka, India.
[2]Department of Humanities and Basic Sciences, Sri Sivani college of Engineering, Chilakapalem, Srikakulam, India

[3]Department of Mathematics, University of Botswana, Gaborone, Botswana

Abstract:

This paper aims to examine the heat transfer enhancement due to convection in Casson hybrid nanofluid flow over a semi-infinite flat plate with thermal diffusion, magnetic field and thermal radiation. In this analysis hybrid nanofluid containing Cobalt, Aluminum oxide $\left(Al_2O_3\right)$ and Ethylene Glycol as base fluid is considered. Equations of the flow model are transformed into dimensionless form and the solutions are obtained for velocity and temperature using the regular perturbation method. The expressions for shear stress and heat transfer rate at the plate are derived. The effects of physical parameters on the flow and derived quantities have been presented in the form of graphs and tables and analyzed. From the results, it is noticed that Casson nanofluid (Cobalt with Ethylene Glycol) exhibits a higher heat transfer rate in comparison with that of Casson hybrid nanofluid.

Keywords: Casson hybrid nanofluid, heat and mass transfer, thermal radiation parameter, thermal diffusion and magnetic field.

Nomenclature

"u,v → x and y components of velocity(m/s)
Q → temperature dependent heat source
β_{hnf} → thermal expansion of hybridnanofluid
μ_{hnf} → viscosity of hybridnanofluid
$(\rho C_p)_{hnf}$ → heat capacitance of the hybridnanofluid
α_{hnf} → thermal diffusivity of the hybridnanofluid
k_{hnf} → thermal conductivity of the hybridnanofluid
k_{s1}, k_{s2} → thermal conductivity of the base fluid
σ_{hnf} → electrical conductivity of the hybridnanofluid
k_{bf} → thermal conductivity of the base fluid
ϕ_1, ϕ_2 → solid volume fraction of nanoparticles
σ_{s1}, σ_{s2} → electrical conductivity of the nanofluid
β → Casson parameter
K → permeability parameter
M → magnetic parameter
S → suction parameter
Gr1 → thermal grashof number
F → radiation parameter
α → angle of inclination
θ → temperature of the hybridnanofluid
Pr → prandtl number
θ_p → primary temperature
θ_s → secondary temperature
u_p → primary velocity
g → acceleration due to gravity
u_s → secondary velocity"

1. Introduction

The transfer of heat in convectional fluids has poor heat transfer capabilities when compared to solid particles. To improve the heat transfer capacity of fluids, we add some solid particles to base fluids. These solid particles are nanoparticles such as Al_2O_3, CuO, TiO_2, etc. Solid particles or nanoparticles with base fluids are called nanofluids. Nanofluid is used to enhance the heat transfer rate among fluids. This procedure was first introduced by Choi [1] in 1995. These nanofluids have numerous applications in industries, biomedical fields, mechanical applications, transportation, etc. Some researchers [2-4] have analysed the effect of thermal conductivity when powered form of Al_2O_3 nanoparticle is added to the base fluid. Xilong et al. [5] studied, experimentally, the impact of heat transfer and mass distribution of nanofluids for various values of magnetic fields by considering the thermal boundary layer and vortex flow. Sudarshan et al. [6] analysed the effect of heat and mass transfer by considering boundary layer flow across a nanofluid in the vertical permeable plate. Kiran Kumar et al. [7-8] have discussed the impact of a chemical reaction and thermo-diffusion on the heat and mass transfer free convective flow of nanofluids in between permeable medium in a rotating frame. Hayat et al. [9] analysed the magnetic field behaviour in Oldroyd-B nanofluid in 3D flow under a new set of boundary conditions. Venkateswarlu and Satyanarayana [10] analysed the impact of heat and mass transfer with chemical reaction and radiation absorption in nanofluids in a rotating system. Mohebbi et al. [11] observed the

behaviour of nanofluids under the influence of an internal heat source in a C-shaped enclosure. Ines Goncalves et al. [12] reviewed the thermal conductivity of the nanofluids where they compared different models and challenges, and they stated that nanofluids have a range of applications from nanomedicine to renewable energies due to their superior thermal properties

Casson fluid comes under the class of non-Newtonian fluid due to its viscoelastic property. Casson fluid at infinite viscosity in the absence of a shear rate is noticed as a shear-thinning liquid. Examples of Casson fluids are soup, blood, honey and orange juice. This type of fluid has applications in food manufacturing, engineering operations and some metallurgical processes [13,14]. Aurang et al. [15] focused on two concepts. One involves a boundary layer Casson fluid movement, while the other is a quick dissipation of viscous fluid caused by heat transfer. Ibukun et al. [16]. studied the impact of heat and mass transport of Casson nanofluid in an unstable stretched sheet in the presence of radiation and internal heat generation. Also, they studied the effects of fluid flow of Soret and Dufour numbers.

Hybrid nanofluids contain two or more nanoparticles suspended in the base fluid. Heat transfer depends upon the properties of base fluids and nanoparticles. The thermal conductivity of nanofluids is low when compared to hybrid nanofluids. Hybrid nanofluids play a major role in industries, as hybrid nanoparticles increase the heat transfer rate and decrease skin friction and thereby decrease production cost [17,18]. By considering spinning cones with variable viscosity, Tulu and Ibrahim [19] discussed the usage of hybrid nanofluids. By considering a hybrid nanofluid, Asifa et al. [20] analysed the rate of heat and mass transfer by rotating discs. Finally, they observed that the enhancement of heat in hybrid nanofluid is more when compared to common fluid. Hassan et al. [21] worked on Jeffery hybrid nanofluids and they studied the effect of radiation parameters and the effect of heat absorption and radiation parameter. The outcome is that the velocity decreases as the magnetic parameter increases.

Motivated by the above literature survey which has numerous applications in the field of science and technology, it is prompted to discuss and study the heat transfer analysis of Casson hybrid nanofluid (Cobalt-Aluminium trioxide with Ethylene Glycol) over an inclined plate fixed in a permeable medium in the presence of thermal radiation and external heat source under oscillating boundary constraints, using perturbation technique.

2. Formulation of the Problem

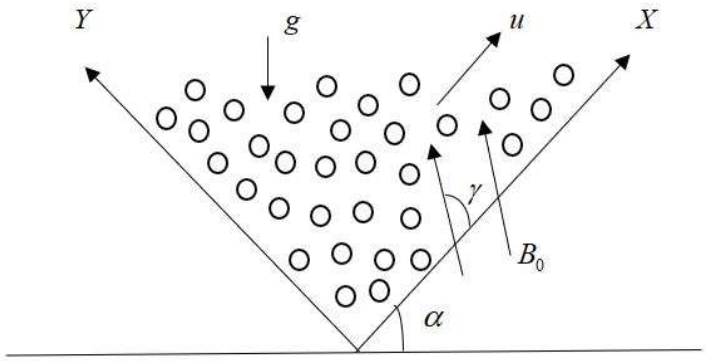

Fig 1: Geometry of the flow model

An unsteady free convectional heat transfer flow of a Casson hybrid nanofluid past an infinite inclined porous moving plate is considered. A rectangular Co-ordinate system is chosen so that the fluid flow direction is along x-direction and y-direction is normal to it. A uniform magnetic field of strength B_0 is applied in the direction of γ with the positive direction of x-axis (as shown in the geometry of the flow model Fig 1). The plate which is along the x-axis makes an α angle with the horizontal line.

Assumptions made during the investigation are:

- Fluid flow parameters are functions of y and t only.
- The induced magnetic field and the applied electric field are neglected because of the polarization of charges.
- The fluid and plate have the same temperature T_∞' when $t \le 0$.
- When $t \ge 0$ the temperature of the plate oscillates harmonically over time with a constant mean.
- Cobalt, Aluminum Oxide – Ethylene Glycol hybrid nanofluid flow under Tiwari – Das model is considered.
- Nanoparticles are uniform in size and shape.

In view of the above-mentioned assumptions, the equations of conservation of mass, momentum and energy equation of the flow model are, respectively,

$$\frac{\partial v'}{\partial y'} = 0 \tag{1}$$

$$\rho_{hnf}\left(\frac{\partial u'}{\partial t'} + v'\frac{\partial u'}{\partial y'}\right) = \mu_{hnf}\left(1+\frac{1}{\beta}\right)\frac{\partial^2 u'}{\partial y'^2} + (\rho\beta)_{hnf}\, g\left(T'-T_\infty'\right)\sin(\alpha) - \frac{\mu_{hmf}u'}{K'} - \sigma_{hmf}B_0^2 u'\sin^2(\gamma) \tag{2}$$

$$\left(\frac{\partial T'}{\partial t'} + v'\frac{\partial T'}{\partial y'}\right) = \frac{k_{hnf}}{\left(\rho C_p\right)_{hnf}}\frac{\partial^2 T'}{\partial y'^2} - \frac{Q'}{\left(\rho C_p\right)_{hnf}}\left(T'-T_\infty'\right) - \frac{1}{\left(\rho C_p\right)_{hnf}}\frac{\partial q_r}{\partial y'} \tag{3}$$

The radiative term is given by

$$q_r = -\frac{4\bar{\sigma}}{3\bar{k}}\frac{\partial T^4}{\partial y'} \tag{4}$$

Here $\bar{\sigma}$ is Stefan Boltzmann constant and $\bar{k}$ is the mean absorption coefficient

$$\frac{\partial q_r}{\partial y'} = -\left(\frac{16\bar{\sigma}T_\infty^3}{3\bar{k}}\right)\frac{\partial^2 T}{\partial y'^2}$$

Boundary conditions for the given problem to solve governing equations are given below:

$$\left.\begin{array}{l} t' \le 0,\ u'(y',t') = 0,\ T' = T_\infty' \\ t' \ge 0,\ u'(y',t') = U_0,\ T' = T_w' + (T_w' - T_\infty')\varepsilon e^{iw't'} \text{ at } y' = 0 \\ u'(y',t') = 0,\ T' = T_\infty' \text{ as } y \to \infty \end{array}\right\} \tag{5}$$

The expressions of the hybrid nanofluids parameters such as density, viscosity, thermal expansion, electric conductivity, electric conductivity, heat capacitance and thermal diffusivity are given as follows:

$$\left.\begin{array}{l} \left(\rho C_p\right)_{hnf} = \left[\left(1-\phi_{s1}\right)\rho_f + \phi_{s1}\rho_{s1}\right]\left(1-\phi_{s2}\right) + \rho_{s2}\phi_{s2}\ , \quad \alpha_{hnf} = \dfrac{k_{hnf}}{\left(\rho C_p\right)_{hnf}} \\ \left(\rho\beta\right)_{hnf} = \left[(1-\phi_{s1})\left(\rho\beta\right)_f + \phi_{s1}\left(\rho\beta\right)_{s1}\right](1-\phi_{s2}) + \left(\rho\beta\right)_{s2}\phi_{s2}\ ,\ \mu_{hnf} = \dfrac{\mu_f}{\sqrt{\left(1-\phi_{s1}\right)^5\left(1-\phi_{s2}\right)^5}} \\ \left(\rho C_p\right)_{hnf} = \left(\rho C_p\right)_f\left(1-\phi_{s2}\right)\left[\left(1-\phi_{s1}\right) + \phi_{s1}\dfrac{\left(\rho C_p\right)_{s1}}{\left(\rho C_p\right)_f}\right] + \phi_2\left(\rho C_p\right)_{s2} \\ \sigma_{hnf} = \sigma_{nf}\left[\dfrac{\sigma_{s2}+2\sigma_{nf}-2\phi_{s2}(\sigma_{nf}-\sigma_{s2})}{\sigma_{s2}+2\sigma_{nf}+\phi_{s2}(\sigma_{nf}-\sigma_{s2})}\right],\ \sigma_{nf} = \sigma_f\left[\dfrac{\sigma_1+2\sigma_f-2\phi_1(\sigma_f-\sigma_1)}{\sigma_1+2\sigma_f+\phi_1(\sigma_f-\sigma_1)}\right] \end{array}\right\} \tag{6}$$

The subscripts nf, f, $s1$ and $s2$ constitute thermophysical properties of the nanofluid, base fluid and nanoparticles respectively.

According to Maxwell thermal conductivity of hybrid nanofluid k_{hnf} is given as:

$$k_{hnf} = k_{bf}\left[\frac{k_{s2}+2k_{bf}-2\phi_2\left(k_{bf}-k_{s2}\right)}{k_{s2}+2k_{bf}+\phi_2\left(k_{bf}-k_{s2}\right)}\right], k_{bf} = k_f\left[\frac{k_{s1}+2k_f-2\phi_1\left(k_f-k_{s1}\right)}{k_{s1}+2k_f+\phi_1\left(k_f-k_{s1}\right)}\right] \tag{7}$$

where, k_{nf}, k_{bf}, k_{s1} and k_{s2} are thermal conductivity of nanofluid, base fluid and nanoparticles respectively.

Thermophysical properties of base fluids and solid nanoparticles are:

property	Ethylene Glycol (EG)	Cobalt (Co)	Aluminium Oxide (Al_2O_3)
$\rho(kg/m^2)$	1114	8900	3970
$k(W/mK)$	0.25	100	40
$C_p(J/kg\ K)$	2415	420	765
σ(Simens/m)	$5.5\times\ 10^{-6}$	$1.602\times\ 10^{7}$	$35\times\ 10^{6}$
$\beta(1/K)$	$57\times\ 10^{-5}$	$1.3\times\ 10^{-5}$	$0.85\times\ 10^{-5}$

The dimensionless parameters used are

$$u=\frac{u'}{U_0},\ y=\frac{U_0 y'}{v_f},\ t=\frac{U_0^2 t'}{v_f},\ w=\frac{v_f w'}{U_0^2},\ \theta=\frac{\left(T'-T_\infty'\right)}{\left(T_w'-T_\infty'\right)},\ S=\frac{v_0}{U_0},$$

$$M=\frac{\sigma B_0^2 v_f}{\rho_f U_0^2},\ Q=\frac{Q' v_f^2}{k_f U_0^2},\ \mathrm{Pr}=\frac{v_f}{\alpha_f},\ K=\frac{K' U_0^2}{v_f^2},\ E=\frac{E_0}{U_0 B_0},\ F=\frac{4T_\infty^3\bar{\sigma}}{k_{hnf}\bar{k}}, \tag{8}$$

$$G_r=\frac{v_f g\left(\rho\beta\right)_f}{\rho_f U_0^3}\left(T_w'-T_\infty'\right), v_f=\frac{\mu_f}{\rho_f}$$

Using the above dimensionless parameters, equations (2), (3) reduce to the following dimensionless form:

$$C\left(\frac{\partial u}{\partial t}-S\frac{\partial u}{\partial y}\right)=\left[D\left(1+\frac{1}{\beta}\right)\frac{\partial^2 u}{\partial y^2}+EGr1\sin(\alpha)\theta-D\frac{u}{K}-F\left(M\sin^2\left(\gamma\right)\right)u\right] \tag{9}$$

$$G\left[\frac{\partial\theta}{\partial t}-S\frac{\partial\theta}{\partial y}\right]=\frac{1}{\mathrm{Pr}}\left[H\left(1+\frac{4F}{3}\right)\frac{\partial^2\theta}{\partial y^2}-Q\theta\right] \tag{10}$$

The non-dimensional boundary conditions are

$$\left.\begin{array}{l} t \le 0 :\ u(y,t) = 0,\ \theta = 0 \\ t \ge 0, u(y,t) = 1, \theta = 1 + \varepsilon e^{iwt} \text{ at } y = 0 \\ u = 0,\ \theta = 0 \text{ as } y \to \infty \end{array}\right\} \quad (11)$$

3. Solution of the problem

To convert the coupled partial differential equations (9) and (10) to a system of linear ordinary differential equations, we form an asymptotic analysis by representing the velocity and temperature as:

$$\left.\begin{array}{l} u(y,t) = u_0(y) + \varepsilon u_1(y) e^{i\omega t} + \ldots\ldots\ldots\ldots \\ \theta(y,t) = \theta_0(y) + \varepsilon \theta_1(y) e^{i\omega t} + \ldots\ldots\ldots\ldots \end{array}\right\} \quad (12)$$

where $(\varepsilon < 1)$ is a parameter

Substituting equations (12) into equations (9), (10) and (11), and equating the like powers of ε and ignoring higher powers of ε, we obtain:

$$H\left(1 + \frac{4F}{3}\right)\theta_0'' + \Pr GS\theta_0' - Q\theta_0 = 0 \quad (13)$$

$$H\left(1 + \frac{4F}{3}\right)\theta_1'' + \Pr GS\theta_1' - \left(Q + \Pr G(i\omega)\right)\theta_1 = 0 \quad (14)$$

$$L_{14}u_0'' + CSu_0' - L_{15}u_0 = -EG_r\theta_0 \quad (15)$$

$$L_{14}u_1'' + CSu_1' - L_{16}u_1 = -EG_r\theta_1 \quad (16)$$

The boundary conditions are reduced to following form:

$$\left.\begin{array}{l} u_0 = 1,\ u_1 = 0,\ \theta_0 = 1,\ \theta_1 = 1 \text{ at } y = 0 \\ u_1 = 0,\ u_0 = 0,\ \theta_0 = 0,\ \theta_1 = 0 \text{ as } y \to \infty \end{array}\right\} \quad (17)$$

Solving equations (13) – (16) under the boundary conditions (17) and using (12), we obtain the expressions for temperature and velocity as follows:

$$\theta(y,t) = \theta_p + i\theta_s \quad (18)$$

$$\text{where, } \theta_p = e^{-L_4 y} + \varepsilon e^{-L_8 y}\cos(L_9 y)\cos(\omega t) + \varepsilon e^{-L_8 y}\sin(L_9 y)\sin(\omega t) \tag{19}$$

$$\theta_s = \left(-\varepsilon e^{-L_8 y}\sin(L_9 y)\cos(\omega t) + \varepsilon e^{-L_8 y}\cos(L_9 y)\sin(\omega t)\right) \tag{20}$$

$$u(y,t) = u_p + iu_s \tag{21}$$

$$\text{where, } u_p = \begin{pmatrix} L_{21}e^{-L_{17}y} \\ +L_{19}e^{-L_4 y} \end{pmatrix} + \varepsilon \begin{bmatrix} L_{35}e^{-L_{28}y}\cos(L_{29}y)\cos(\omega t) + L_{35}e^{-L_{28}y}\sin(L_{29}y)\cos(\omega t) \\ +L_{34}e^{-L_{28}y}\sin(L_{29}y)\cos(\omega t) - L_{34}e^{-L_{28}y}\cos(L_{29}y)\sin(\omega t) \\ +L_{33}e^{-L_8 y}\cos(L_9 y)\cos(\omega t) + L_{33}e^{-L_8 y}\sin(L_9 y)\sin(\omega t) \\ -L_{34}e^{-L_8 y}\sin(L_{34}y)\cos(\omega t) + L_{34}e^{-L_8 y}\cos(L_{34}y)\sin(\omega t) \end{bmatrix} \tag{22}$$

$$u_s = \varepsilon \begin{pmatrix} -L_{35}e^{-L_{28}y}\sin(L_{29}y)\cos(\omega t) + L_{35}e^{-L_{28}y}\cos(L_{29}y)\sin(\omega t) \\ +L_{34}e^{-L_{28}y}\cos(L_{29}y)\cos(\omega t) + L_{34}e^{-L_{28}y}\sin(L_{29}y)\sin(\omega t) \\ -L_{33}e^{-L_8 y}\sin(L_9 y)\cos(\omega t) + L_{33}e^{-L_8 y}\cos(L_9 y)\sin(\omega t) \\ -L_{34}e^{-L_8 y}\cos(L_{34}y)\cos(\omega t) - L_{34}e^{-L_8 y}\sin(L_{34}y)\sin(\omega t) \end{pmatrix} \tag{23}$$

From science and technology point of view, the skin friction $\left(C_f\right)$ coefficient and the Nusselt number $\left(Nu\right)$ are important characteristics of the flow.

The skin-friction co-efficient (primary and secondary) at the plate $y = 0$ is given by:

$$C_f = \left(u_p'\right)_{y=0} + i\left(u_s'\right)_{y=0} \tag{24}$$

$$\left|C_f\right| = \sqrt{\left(u_p'\right)_{y=0}^2 + i\left(u_s'\right)_{y=0}^2} \tag{25}$$

$$\text{where, } \left(u_p'\right)_{y=0} = \begin{pmatrix} L_{21}(-L_{17}) \\ +L_{19}(-L_4) \end{pmatrix} + \varepsilon \begin{bmatrix} L_{35}(-L_{28})\cos(\omega t) + L_{35}(L_{29})\cos(\omega t) + L_{34}(L_{29})\cos(\omega t) \\ +L_{34}(L_{28})\sin(\omega t) - L_{33}L_8\cos(\omega t) + L_{33}L_9\sin(\omega t) \\ -(L_{34})^2\cos(\omega t) - L_{34}L_8\sin(\omega t) \end{bmatrix} \tag{26}$$

$$\left(u_s'\right)_{y=0} = \varepsilon \begin{bmatrix} -L_{35}L_{29}\cos\left(\omega t\right) + L_{35}(-L_{28})\sin\left(\omega t\right) + L_{34}(-L_{28})\cos(\omega t) + L_{34}L_{29}\sin(\omega t) \\ -L_{33}L_9\cos(\omega t) + L_{33}(-L_8)\sin(\omega t) + L_{34}L_8\cos(\omega t) - L_{34}^2\sin(\omega t) \end{bmatrix} \tag{27}$$

The Nusselt number (primary and secondary) at the plate $y = 0$ is given by:

$$Nu = -\left(\left(\theta_p'\right)_{y=0} + i\left(\theta_s'\right)_{y=0}\right) \tag{28}$$

$$|Nu| = \sqrt{\left(\theta_p^{'}\right)_{y=0}^{2} + i\left(\theta_s^{'}\right)_{y=0}^{2}} \tag{29}$$

where, $-\left(\theta_p^{'}\right)_{y=0} = \left(L_4 + \varepsilon L_8 \cos(\omega t) - \varepsilon L_9 \sin(\omega t)\right)$ (30)

$$-\left(\theta_s^{'}\right)_{y=0} = \left(\varepsilon L_9 \cos(\omega t) + \varepsilon L_8 \sin(\omega t)\right) \tag{31}$$

4. Results and discussions

The solutions are carried out for various physical parameters like suction parameter, magnetic parameter, radiation parameter and Casson parameter etc. on heat transfer and flow of Casson hybrid nanofluid over an inclined porous infinite plate. The above several parameters' equations are used in MATLAB to produce figures 2 to 41.

- **Effect of Suction parameter**

The impact of suction parameter S on the fluid for primary and secondary velocities and primary and secondary temperatures for both Casson hybrid nanofluid and Casson nanofluid is shown in graphs. From the graphs, it is seen that the primary temperature of Casson hybrid nanofluid and Casson nanofluid decreases by increasing the Suction parameter.

From Fig 2 and Fig 3, it is noticed that the primary temperature of Casson hybrid nanofluid is high when compared to Casson nanofluid, and a reverse phenomenon is observed in the secondary temperature. The trend shows that the temperature decreases with an increase in the suction parameters. i.e., temperature distribution across the boundary layer flow decreases with an increase in the suction parameter. From Fig 4 and Fig 5, the effects of primary and secondary velocity on the suction parameter can be noted. The velocity decreases as the suction parameter increases. This effect is seen in both velocities (primary and secondary). This is because suction sustains the boundary growth.

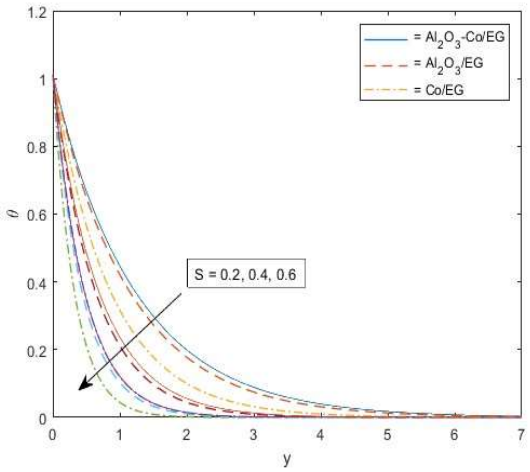

Fig 2: Profiles of θ_p for different S

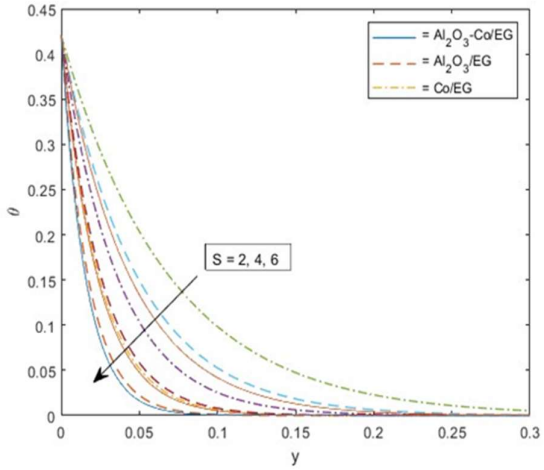

Fig 3: Profiles of θ_s for different S

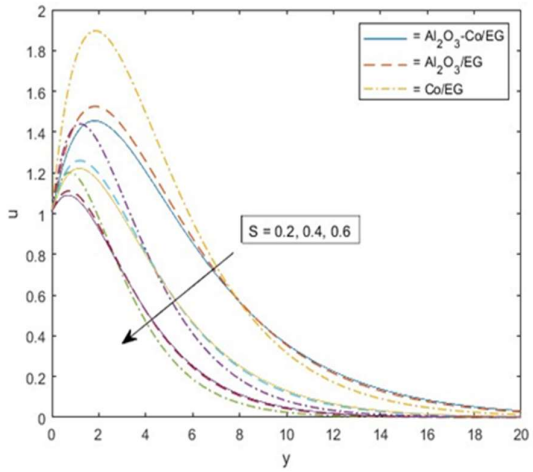

Fig 4: Profiles of u_p for different S

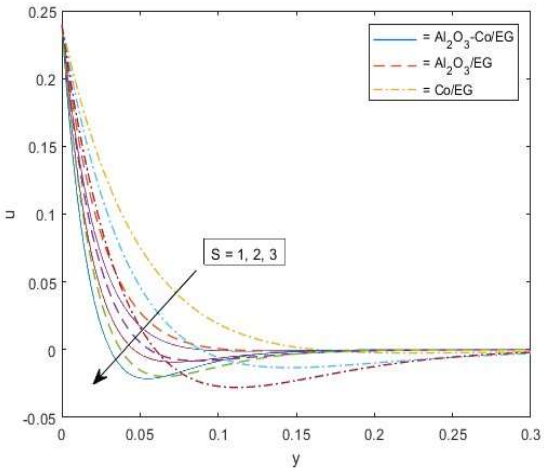

Fig 5: Profiles of u_s for different S

- **Effect of Magnetic field**

The influence of magnetic field parameter (M) on boundary layer flow is observed in Fig 6 and Fig 7, for hybrid nanofluid and nanofluid. The velocity (primary and secondary) is higher for the Casson nanofluid. Primary and secondary velocities decrease as increasing the values of a magnetic parameter. Physically it meets the logic that the magnetic field is a Lorentz force, it extorts a retarding force on flow.

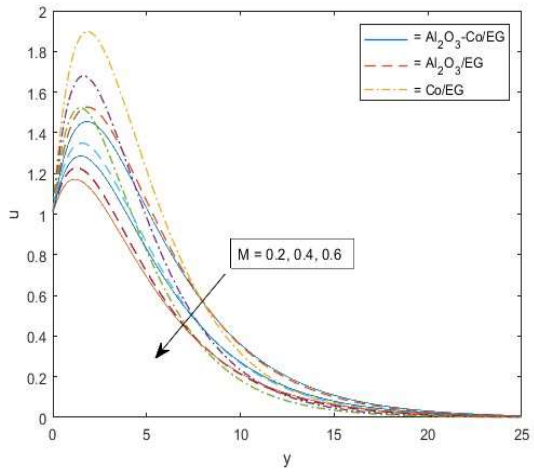

Fig 6: Profiles of u_p for different M

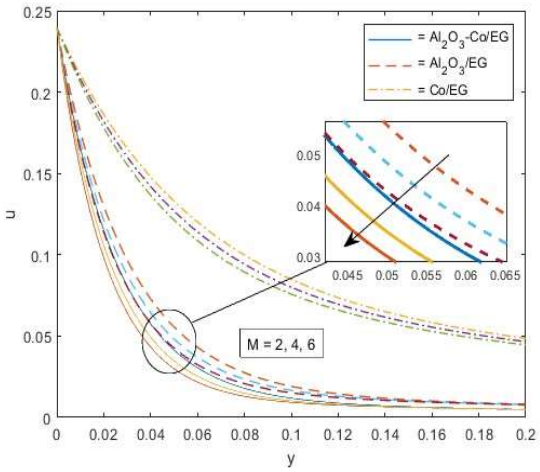

Fig 7: Profiles of u_s for different M

- **Effect of Radiation**

The effect of radiation parameter (F) on fluid flow is displayed in Fig 8 and Fig 9. From the graphs, it is observed that the thermal boundary layer is thick in Casson hybrid nanofluid when compared to Casson nanofluid in primary temperature case. It is noticed that the primary temperature increases as radiation increases. A reverse effect is noticed in secondary temperature. Physically this means that the fluid temperature can be controlled by radiation.

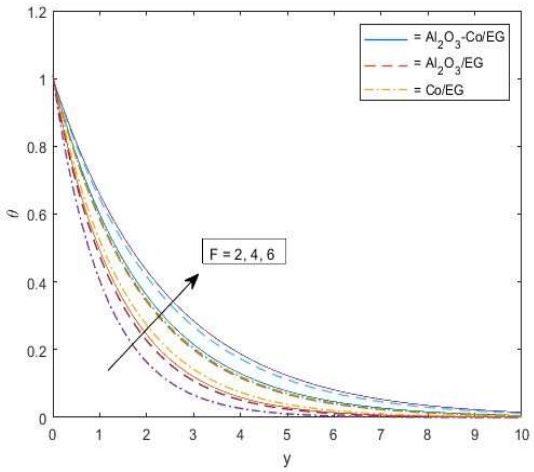

Fig 8: Profiles of θ_p for different F

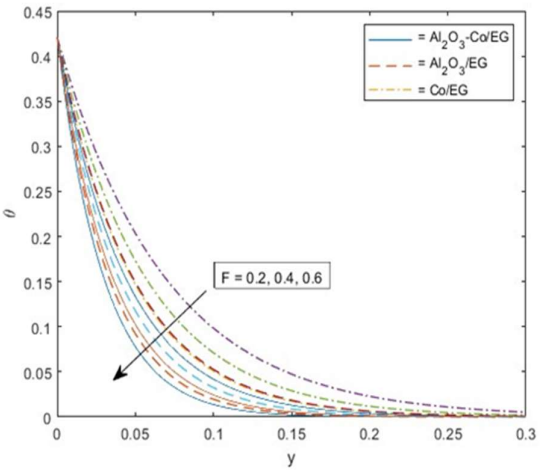

Fig 9: Profiles of θ_s for different F

Fig 10 and Fig 11 represent velocity variation with radiation parameter. It is observed that the velocity of Casson nanofluid is greater when compared to Casson hybrid nanofluid in both

primary and secondary velocities. As radiation increases, the primary velocity increases. It is observed a reverse phenomenon in secondary velocity.

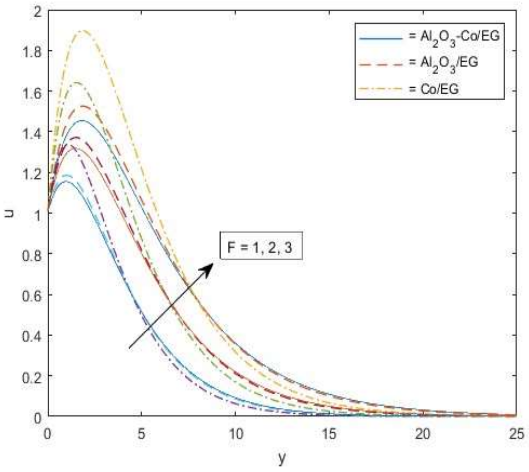

Fig 10: Profiles of u_p for different F

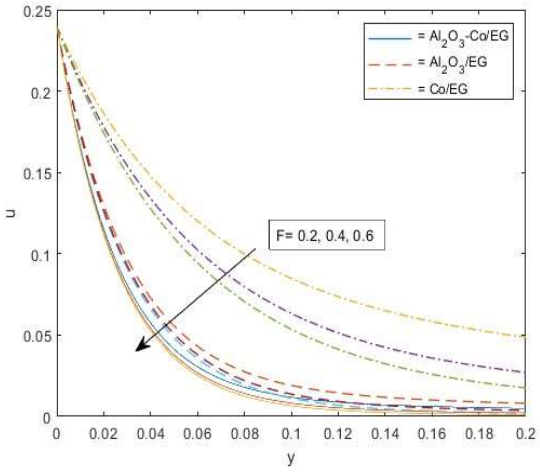

Fig 11: Profiles of u_s for different F

- **Effect of Casson parameter**

Fig 12 and Fig 13 depicts the effects of Casson parameter β on velocity for Casson hybrid nanofluid and Casson nanofluid. The velocity of Casson nanofluid is higher when compared to Casson hybrid nanofluid. Boundary layer thickness increases as Casson parameter increases in secondary velocity. The velocity of Casson nanofluid is high when compared to Casson hybrid nanofluid. Physically it means that Casson creates resistance in a liquid stream.

In Fig 12 it is noticed that the velocity of Casson hybrid nanofluid is high and a reverse phenomenon is seen at the point y=5.9. Also, for Casson nanofluid (Aluminium trioxide with Ethylene glycol) the reverse process is seen at the point y=6.03, and also the reverse process is observed at the point y=6.08 for Casson nanofluid (Cobalt with Ethylene Glycol).

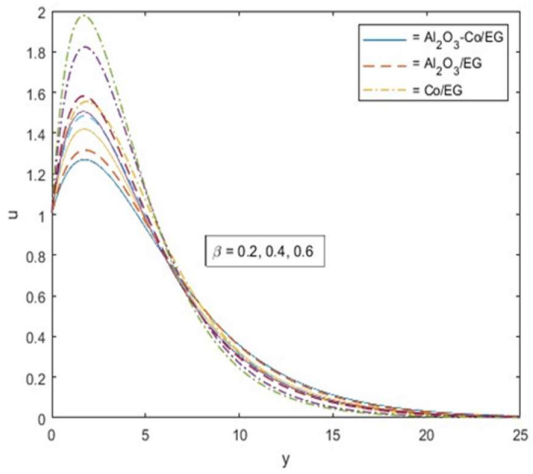

Fig 12: Profiles of u_p for different β

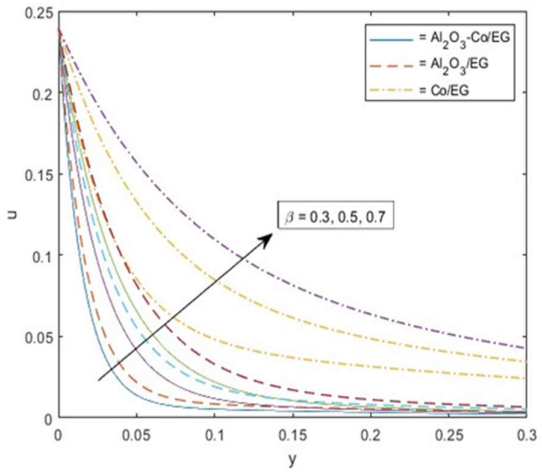

Fig 13: Profiles of u_s for different β

- **Effects of Heat Generation and Absorption**

The behaviour of heat absorption and generation in relation to velocity and temperature is shown in Figs. 14–18. The velocity and temperature of the thermal boundary layer thickness drops as the heat absorption rises. Fig 19 and Fig 20 show the effect of heat generation on primary temperature and velocity. It is noticed that there is fluctuation in both velocity and temperature near the plate. This effect is seen for both Casson hybrid nanofluid and Casson nanofluid.

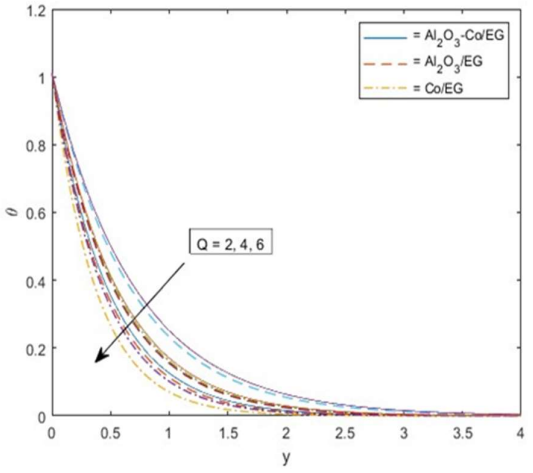

Fig 14: Profiles of θ_p for different Q

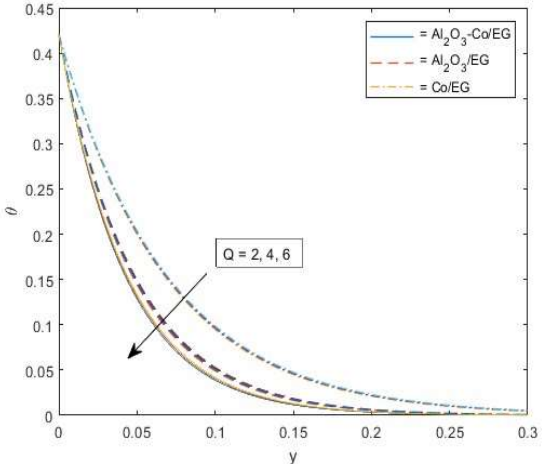

Fig 15: Profiles of θ_s for different Q

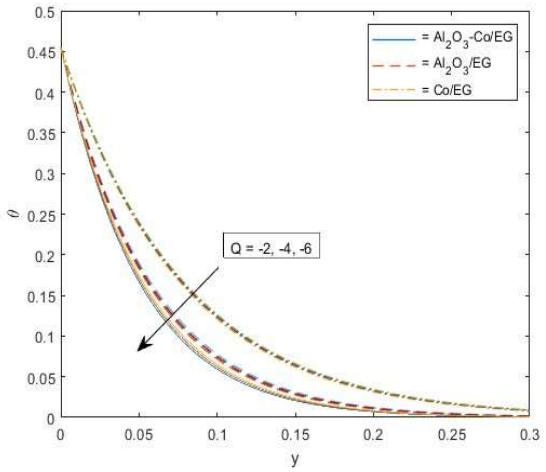

Fig 16: Profiles of θ_s for different Q

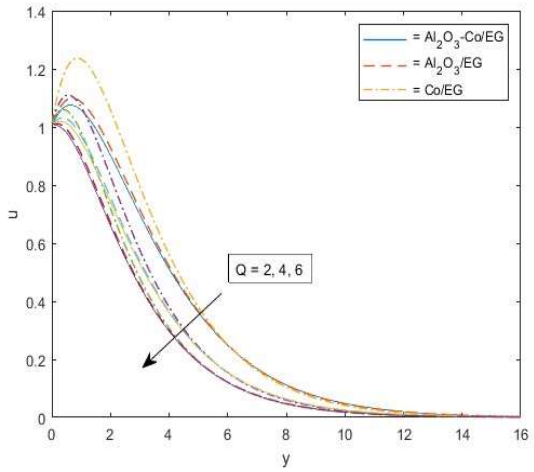

Fig 17: Profiles of u_p for different Q

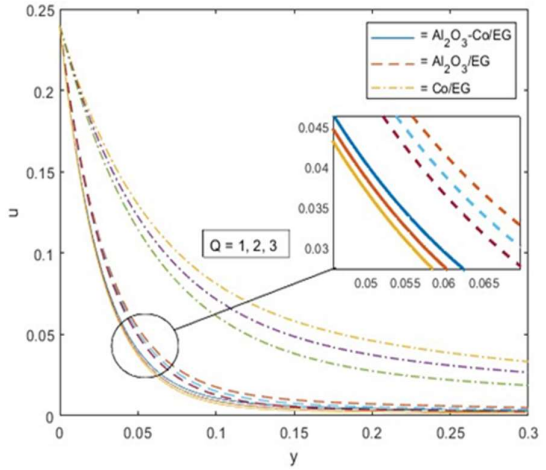

Fig 18: Profiles of u_s for different Q

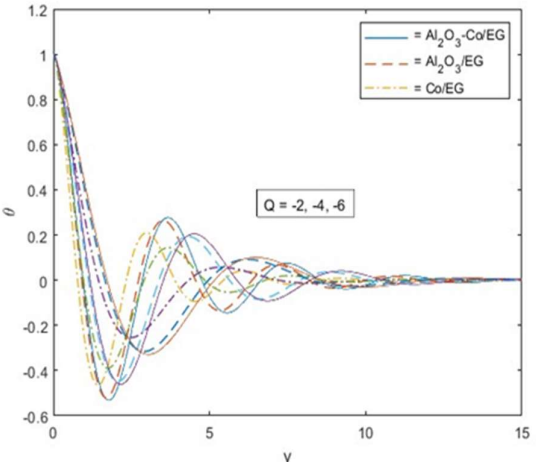

Fig 19: Profiles of θ_p for different Q

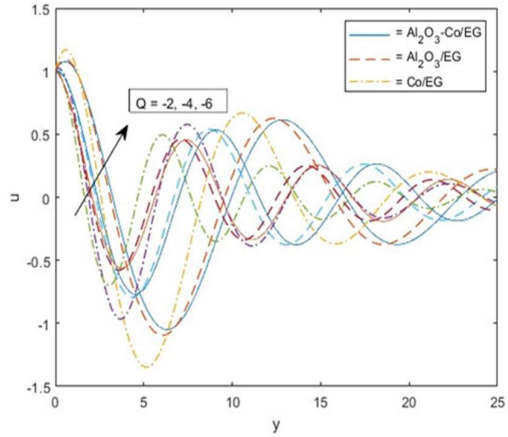

Fig 20: Profiles of u_p for different Q

- **Effect of Grashof number**

The effect of Grashof number on primary velocity and secondary velocity is discussed in Fig 21 and Fig 22. The velocity of Casson nanofluid is more when compared to Casson hybrid nanofluid. It is noticed that the primary and secondary velocities increase with an increment in Grashof number. This is due to the inertia and buoyancy effect of fluid flow due to natural convection.

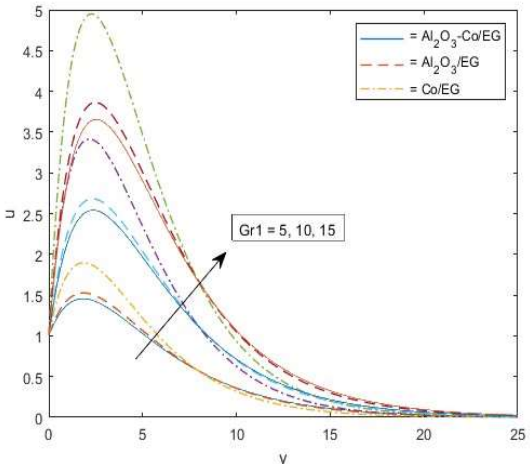

Fig 21: Profiles of u_p for different $Gr1$

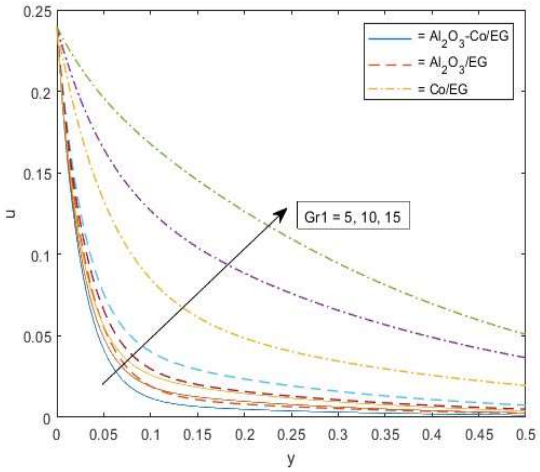

Fig 22: Profiles of u_s for different $Gr1$

- **Effect of Porous parameter**

Fig 23 and Fig 24 represent the velocity profile for different values of porous parameter. The velocity of Casson nanofluid is high when compared to Casson hybrid nanofluid. Velocity increases as the porous parameter increases. This is due to the effect of permeable medium on the boundary layer development because of the expansion in thickness of the momentum boundary layer.

- **Effect of Inclined angle**

The effect of inclined angle can be seen in Fig 25 and Fig 26. It is observed that the flow rate of Casson nanofluid is more in both cases. Velocity increases as the angle of inclination increases. Here, higher gravitational effects cause fluid to travel at a higher velocity.

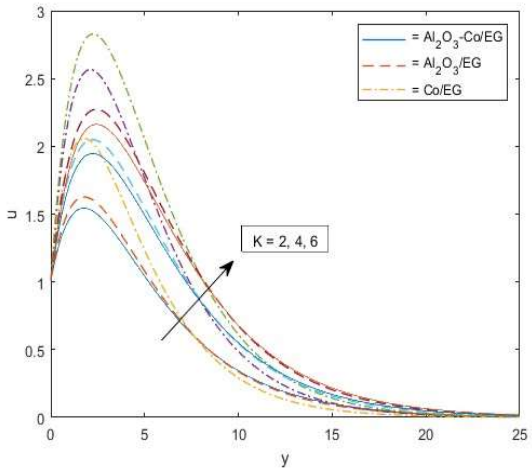

Fig 23: Profiles of u_p for different K

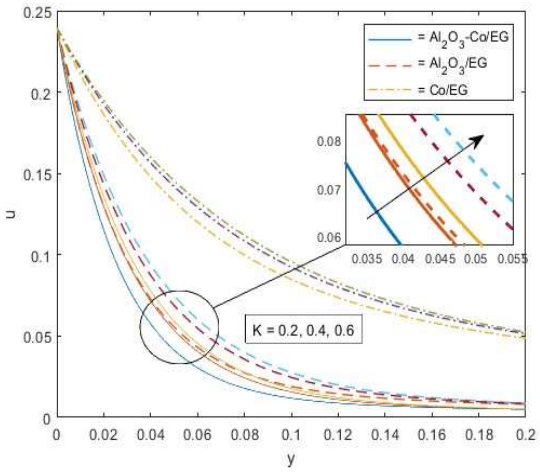

Fig 24: Profiles of u_s for different K

- **Effect of Aligned angle**

The effect of Aligned magnetic field can be observed in Fig 27 and Fig 28. It is found that the velocity can be reduced by increasing the value of Aligned angle. The velocity of the Casson nanofluid is more when compared to Casson hybrid nanofluid due to high thermal conductivity of Cobalt.

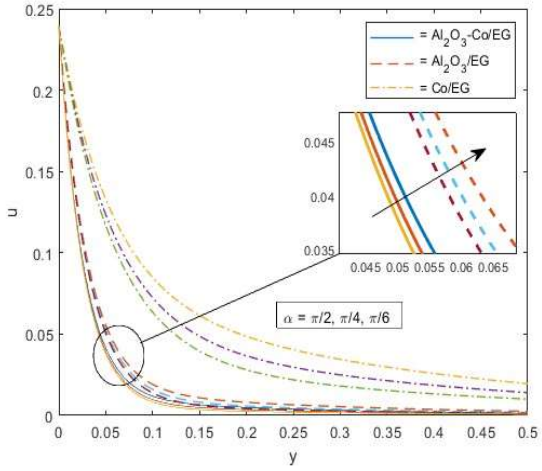

Fig 25: Profiles of u_p for different α

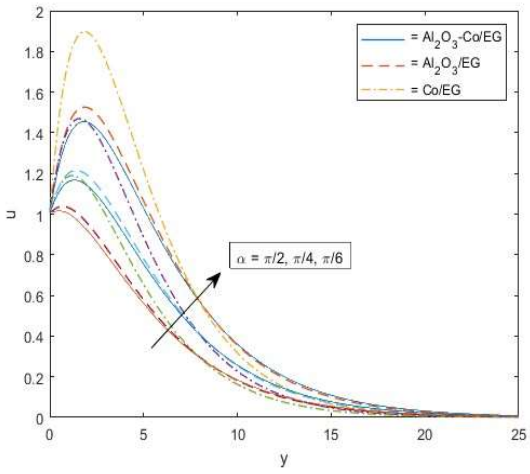

Fig 26: Profiles of u_s for different α

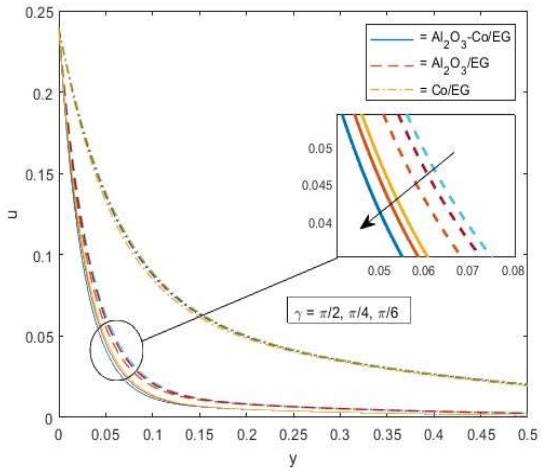

Fig 27: Profiles of u_s for different γ

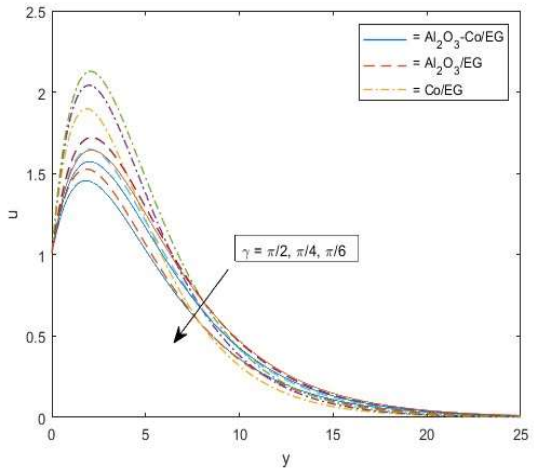

Fig 28: Profiles of u_p for different γ

Fig 29 shows that the temperature decreases as the heat absorption parameter increases. The temperature fluctuates as heat radiation parameter increases. The temperature increases as thermal radiation parameter increases. This effect is observed in Fig 30 in the absence of a heat absorption parameter.

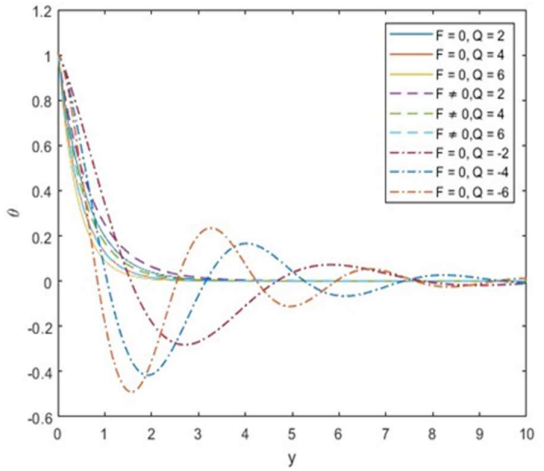

Fig 29: Profiles of θ_p for different F and Q

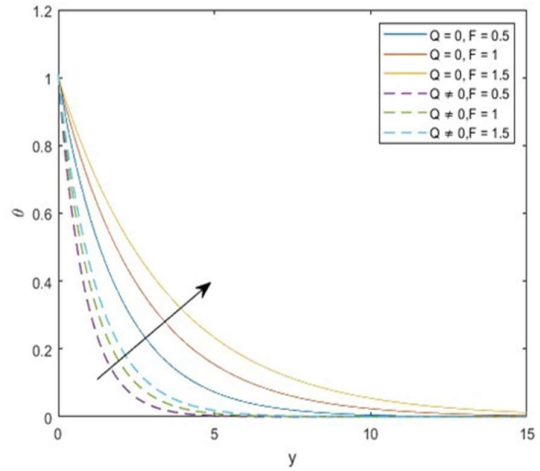

Fig 30: Profiles of θ_p for different F and Q

- **Effect of frequency ω and t on temperature**

From Fig 31 it is seen that the effect of ω on primary temperature is more for Casson hybrid nanoparticles. As frequency ω increases, temperature decreases. In Fig 32, it is observed that the secondary temperature is more for Casson nanofluids. Secondary temperature

increases as frequency ω increases. From Fig 33 and Fig 34, it is noticed that the temperature is high for Casson hybrid nanofluid than for Casson nanofluid in the case of primary temperature. Temperature is high for Casson nanofluid in the case of secondary temperature. In both cases, temperature decreases as time varies.

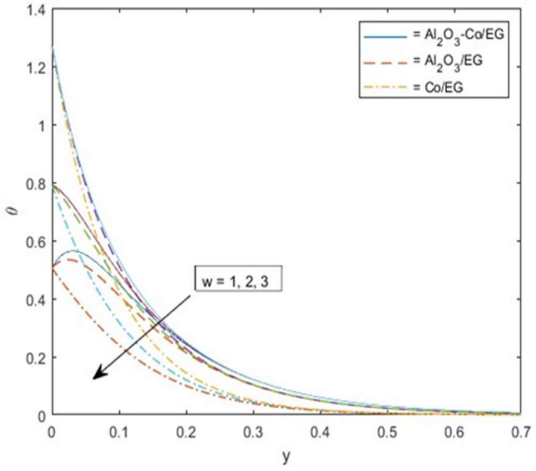

Fig 31: Profiles of θ_p for different ω

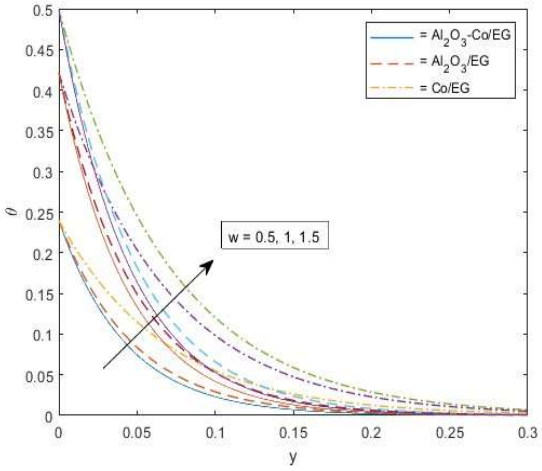

Fig 32: Profiles of θ_s for different ω

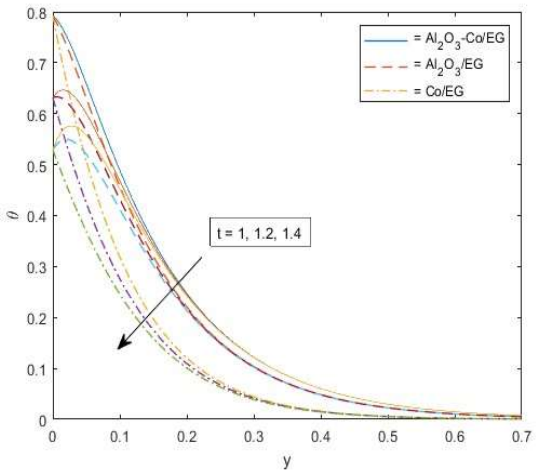

Fig 33: Profiles of θ_p for different time

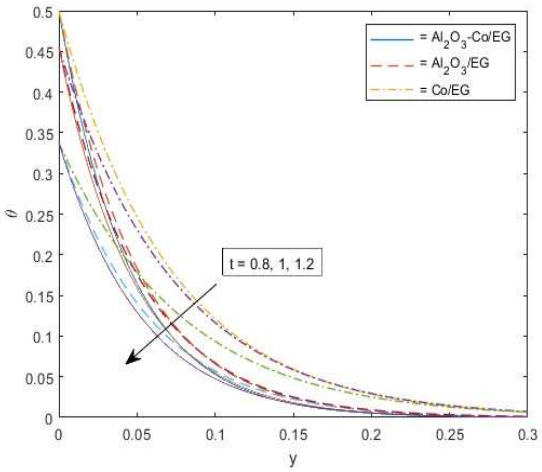

Fig 34: Profiles of θ_s for different time

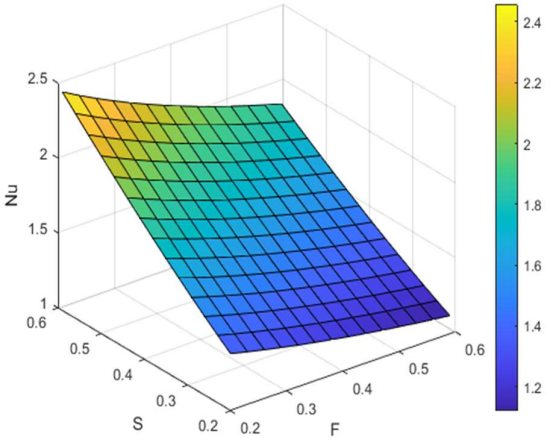

Fig 35: Nusselt number verses F and S

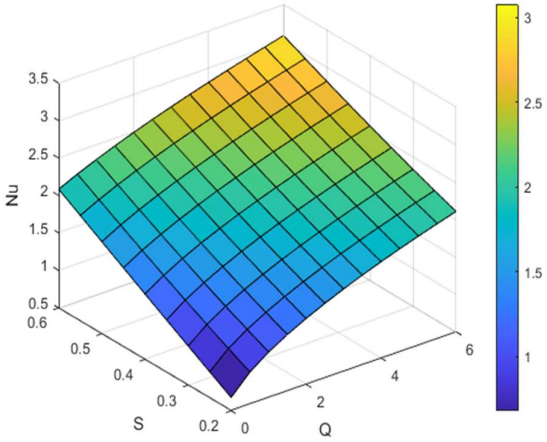

Fig 36: Nusselt number verses Q and S

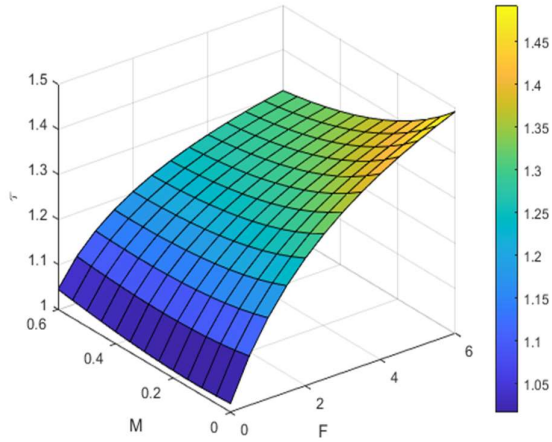

Fig 37: Skin friction verses F and M

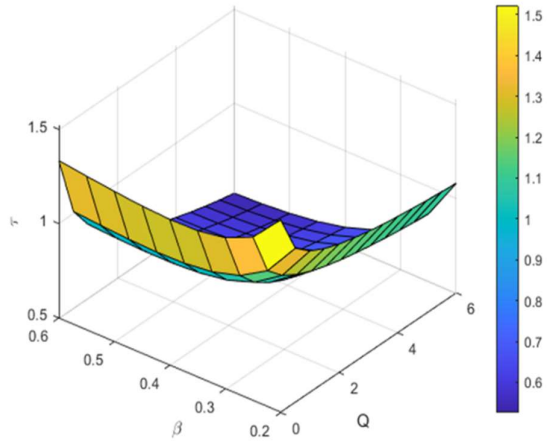

Fig 38: Skin friction verses β and Q

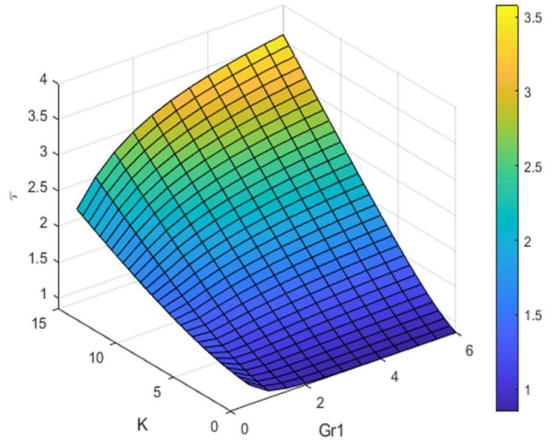

Fig 39: Skin friction verses K and Gr1

The effect of Nusselt number for Casson hybrid nanofluid is observed from Fig 35 and 36. It is noticed that by increasing heat radiation parameter and suction parameter heat transfer rate can be enhanced. Heat transfer rate decreases as the radiation parameter increases. Rate of heat transfer is high when Suction and heat radiation parameter increases when compared to radiation parameter and this effect is observed due to the High thermal conductivity of Cobalt nanoparticles.

From Fig 37 – Fig 39, it is observed that the Skin friction coefficient decreases as heat absorption and magnetic parameters increase. The Skin friction coefficient increases as radiation parameter, porous parameter and Grashof number parameter are increased. Skin friction coefficient vary as the Casson parameter increases.

5. Validation of results:

Comparative study of the present work with that of Vedavathi et al. [23] is shown in Fig 40 and Fig 41. It is observed that the velocity profiles of the present study when β =0 and F=0 are in good agreement with those of Vedavathi et al. when Du=0 and Q_L=0.

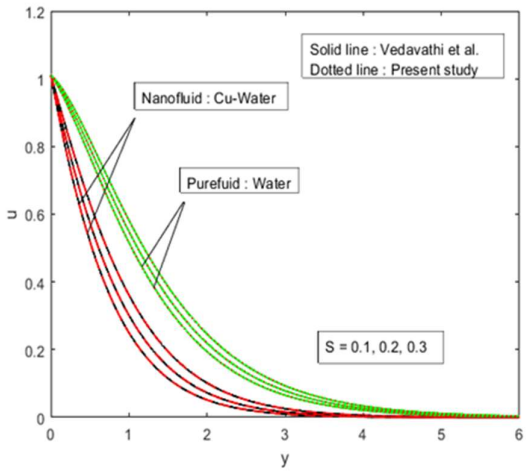

Fig 40: Profiles of u for different S

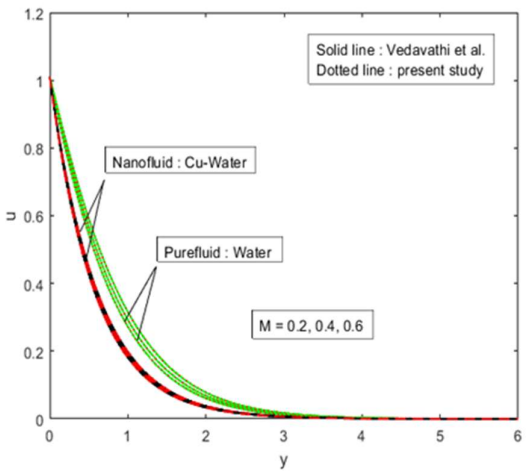

Fig 41: Profiles of u for different M

6. Conclusions

In this work, the convective heat transfer flow of a Casson hybrid nanofluid through a porous media bounded by a semi-infinite flat plate has been examined in the presence of thermal radiation, thermal diffusion and magnetic field. The standard perturbation approach is used to solve the dimensionless equations. The impact of different material parameters on velocity, temperature, skin friction and the heat transfer rate at the plate are presented and studied.

Some main conclusions from this study are:

- Fluid velocity in the boundary layer region reduces when the Suction parameter increases for $EG / Al_2O_3 - Co$, EG / Al_2O_3 and EG / Co whereas it increases with the permeability parameter, Casson parameter, and radiation parameter.
- Magnetic parameter (M) increases as velocity decreases.
- As the Grashof number increases, thickness of thermal boundary layer increases.
- Enhancement of heat transfer rate is high in Casson nanofluid (Cobalt with Ethylene Glycol) than that of in Casson hybrid nanofluid.

References:

1) Choi, S U.S., and Eastman, J A, "Enhancing thermal conductivity of fluids with nanoparticles". United States, 1995, https://www.osti.gov/servlets/purl/196525.
2) S. K. Das, N. Putra, P. Thiesen, and W. Roetzel, “Temperature dependence of thermal conductivity enhancement for nanofluids,” *J Heat Transfer*, vol. 125, no. 4, pp. 567–574, Aug. 2003, doi: 10.1115/1.1571080.
3) N. Putra, W. Roetzel, and S. K. Das, “Natural convection of nano-fluids,” *Heat and Mass Transfer*, vol. 39, no. 8–9, pp. 775–784, Sep. 2003, doi: 10.1007/s00231-002-0382-z.
4) C.H. Chon, K. D. Kihm, S. P. Lee, and S. U. Choi, “Empirical correlation finding the role of temperature and particle size for nanofluid (Al2O3) thermal conductivity enhancement”, *Applied Physics*, vol. 87(15), pp. 153107, 2005.
5) X. Zhang and Y. Zhang, “Experimental study on enhanced heat transfer and flow performance of magnetic nanofluids under alternating magnetic field,” *International Journal of Thermal Sciences*, vol. 164, Jun. 2021, doi: 10.1016/j.ijthermalsci.2021.106897.
6) P. S. Reddy, P. Sreedevi, and A. J. Chamkha, “Heat and Mass Transfer Flow of a Nanofluid over an Inclined Plate under Enhanced Boundary Conditions with Magnetic Field

and Thermal Radiation," *Heat Transfer - Asian Research*, vol. 46, no. 7, pp. 815–839, Nov. 2017, doi: 10.1002/htj.21245.

7) R. V. M. S. S. Kiran Kumar, P. Durga Prasad, and S. V. K. Varma, "Analytical Study of Heat and Mass Transfer Enhancement in Free Convection Flow with Chemical Reaction and Constant Heat Source in Nanofluids," in *Procedia Engineering*, 2015, vol. 127, pp. 978–985. doi: 10.1016/j.proeng.2015.11.446.
8) R. Kiran Kumar, Pd. Prasad, and S. Varma, "Thermo-diffusion and Chemical Reaction Effects on Free Convective Heat and Mass Transfer Flow of Conducting Nanofluid Through Porous Medium in a Rotating frame." *Global Journal of Pure and Applied Mathematics*, vol. 12, pp. 342–351, 2016.
9) T. Hayat, T. Muhammad, S. A. Shehzad, M. S. Alhuthali, and J. Lu, "Impact of magnetic field in three-dimensional flow of an Oldroyd-B nanofluid," *J Mol Liq*, vol. 212, pp. 272–282, Dec. 2015, doi: 10.1016/j.molliq.2015.09.023.
10) B. Venkateswarlu and P. v. Satya Narayana, "Chemical reaction and radiation absorption effects on the flow and heat transfer of a nanofluid in a rotating system," *Applied Nanoscience (Switzerland)*, vol. 5, no. 3, pp. 351–360, Mar. 2015, doi: 10.1007/s13204-014-0324-3.
11) R. Mohebbi, M. Izadi, and A. J. Chamkha, "Heat source location and natural convection in a C-shaped enclosure saturated by a nanofluid," *Physics of Fluids*, vol. 29, no. 12, Dec. 2017, doi: 10.1063/1.4993866.
12) Ines Goncalves, Reinaldo Souza and Goncalo Coutinho, "Thermal conductivity of nanofluids: A review on prediction models, controversies and challenges," *Applied Sciences (Switzerland)*, vol. 11, no. 6. MDPI AG, Mar. 02, 2021. doi: 10.3390/app11062525.
13) Wasim Jamshed, Suriya Uma Devi S, Rabia Safar, Fares Redouane, KottakkaranSooppy Nisar and Mohammed R. Eid. "Comprehensive analysis on copper-iron (II, III)/oxide-engine oil Casson nanofluid flowing and thermal features in parabolic through solar collector", *Journal of Taibah University for Science*, vol. 15(1), pp. 619-636, 2021.
14) H. Alotaibi, S. Althubiti, M. R. Eid, and K. L. Mahny, "Numerical treatment of MHD flow of casson nanofluid via convectively heated non-linear extending surface with viscous dissipation and suction/injection effects," *Computers, Materials and Continua*, vol. 66, no. 1, pp. 229–245, 2021, doi: 10.32604/cmc.2020.012234.
15) A. Zaib, K. Bhattacharyya, M. S. Uddin, and S. Shafie, "Dual Solutions of Non-Newtonian Casson Fluid Flow and Heat Transfer over an Exponentially Permeable Shrinking Sheet

with Viscous Dissipation," *Modelling and Simulation in Engineering*, vol. 2016, 2016, doi: 10.1155/2016/6968371.

16) I. S. Oyelakin, S. Mondal, and P. Sibanda, "Unsteady Casson nanofluid flow over a stretching sheet with thermal radiation, convective and slip boundary conditions," *Alexandria Engineering Journal*, vol. 55, no. 2, pp. 1025–1035, Jun. 2016, doi: 10.1016/j.aej.2016.03.003.

17) T. Hayat, S. Nadeem, and A. U. Khan, "Numerical analysis of Ag-CuO/water rotating Hybrid nano fuid with heat generation/absorption." [Online]. Available: https://mc06.manuscriptcentral.com/cjp-pubs

18) D. Gopal, S. H. S. Naik, N. Kishan, and C. S. K. Raju, "The impact of thermal stratification and heat generation/absorption on MHD carreau nano fluid flow over a permeable cylinder," *SN Appl Sci*, vol. 2, no. 4, Apr. 2020, doi: 10.1007/s42452-020-2445-5.

19) A. Tulu and W. Ibrahim, "Mixed convection hybrid nanofluids flow of MWCNTs–Al2O3/engine oil over a spinning cone with variable viscosity and thermal conductivity," *Heat Transfer*, vol. 50, no. 4, pp. 3776–3799, Jun. 2021, doi: 10.1002/htj.22051.

20) A. Tassaddiq *et al.*, "Heat and mass transfer together with hybrid nanofluid flow over a rotating disk," *AIP Adv*, vol. 10, no. 5, May 2020, doi: 10.1063/5.0010181.

21) H. Waqas, U. Farooq, D. Liu, M. Abid, M. Imran, and T. Muhammad, "Heat transfer analysis of hybrid nanofluid flow with thermal radiation through a stretching sheet: A comparative study," *International Communications in Heat and Mass Transfer*, vol. 138, p. 106303, Nov. 2022, doi: 10.1016/j.icheatmasstransfer.2022.106303.

22) P. Durga Prasad, R.V.M.S.S. Kiran Kumar, S.V.K. Varma, "Heat and mass transfer analysis for the MHD flow of nanofluid with radiation absorption*," Ain Shams Engineering Journal,* p. 2090-4479, April. 2016, doi: 10.1016/j.asej.2016.04.016.

23) N. Vedavathi, G. Dharmaiah, K. S. Balamurugan and J. Prakash, "Heat transfer on MHD nanofluid flow over a semi-infinite plate embedded in a porous medium with radiation absorption, heat source and diffusion thermos effect*," Frontiers in heat and mass transfer*, vol. 9, no. 38, 2017, doi: 10.5098/hmt.9.38.

APPENDIX:

$$A=\left[\frac{k_{s1}+2k_f-2\phi_1\left(k_f-k_{s1}\right)}{k_{s1}+2k_f+\phi_1\left(k_f-k_{s1}\right)}\right], G=\left(\left(1-\phi_2\right)\left[\left(1-\phi_1\right)+\phi_1\frac{\left(\rho C_p\right)_{s1}}{\left(\rho C_p\right)_f}\right]+\phi_2\left(\rho C_p\right)_{s2}\right),$$

$$L_3=L_2\left(1+\frac{4F}{3}\right), H=A\left[\frac{k_{s2}+2Ak_f-2\phi_2\left(Ak_f-k_{s2}\right)}{k_{s2}+2Ak_f+\phi_2\left(Ak_f-k_{s2}\right)}\right], L_4=-\left(\frac{P_rGS+\sqrt{\left(P_rGS\right)^2+4L_3Q}}{2L_3}\right)$$

$$L_6=-\left(\frac{\Pr GS+\sqrt{\left(\Pr GS\right)^2+4\left(L_3\left(Q+\Pr Gi\omega\right)\right)}}{2L_3}\right), D=\frac{1}{\sqrt{\left(1-\phi_1\right)^5\left(1-\phi_2\right)^5}}, L_{14}=D\left(1+\frac{1}{\beta}\right)$$

$$L_8=\frac{1}{2L_3}\sqrt{\left(\left(\Pr GS\right)^2+2L_3Q+\sqrt{\left(\Pr GS\right)^4+\left(2L_3Q\right)^2+4\left(\Pr GS\right)^2\left(L_3Q\right)+4\left(G\Pr L_3\omega\right)^2}\right)}$$

$$L_9=\frac{1}{2L_3}\left(\sqrt{\left(-\left(\Pr GS\right)^2-2L_3Q+\sqrt{\left(\Pr GS\right)^4+\left(2L_3Q\right)^2+4\left(\Pr GS\right)^2\left(L_3Q\right)+4\left(G\Pr L_3\omega\right)^2}\right)}\right)$$

$$B=\left[\frac{\sigma_1+2\sigma_f-2\phi_1(\sigma_f-\sigma_1)}{\sigma_1+2\sigma_f+\phi_1(\sigma_f-\sigma_1)}\right], \quad C=[(1-\phi_1)+\phi_1\frac{\rho_{s1}}{\rho_f}](1-\phi_2)+\frac{\rho_{s2}}{\rho_f}\phi_2, \quad L_{15}=\left(\frac{D}{k}+FM_1\right)$$

$$E=[(1-\phi_1)+\phi_1\frac{\left(\rho\beta\right)_{s1}}{\left(\rho\beta\right)_f}](1-\phi_2)+\frac{\left(\rho\beta\right)_{s2}}{\left(\rho\beta\right)_f}\phi_2, \; F=B\left[\frac{\sigma_2+2B\sigma_f-2\phi_2(B\sigma_f-\sigma_2)}{\sigma_2+2B\sigma_f+\phi_2(B\sigma_f-\sigma_2)}\right], L_{27}=C\omega$$

$$L_{16}=\left(\frac{D}{k}+L_{11}M_1+C(i\omega)\right), L_{17}=-\left(\frac{CS+\sqrt{\left(CS\right)^2+4L_{14}L_{15}}}{2L_{14}}\right), L_{19}=\frac{-EG_r}{L_{14}L_4{}^2-CSL_4-L_{15}}$$

$$L_{21}=1-L_{19} \quad L_{22}=-\left(\frac{CS+\sqrt{\left(CS\right)^2+4L_{14}L_{16}}}{2L_{14}}\right) \quad L_{24}=\frac{-EG_r}{L_{14}L_6{}^2-CSL_6-L_{16}} \quad L_{25}=1-L_{24}$$

$$L_{26}=\frac{D}{k}+FM_1, L_{33}=\frac{L_{30}L_{31}}{L_{31}{}^2+L_{32}{}^2}, \; L_{34}=\frac{L_{30}L_{32}}{L_{31}{}^2+L_{32}{}^2}, \; L_{35}=1-L_{33}$$

$$L_{28}=\frac{1}{2L_{14}}\left[\sqrt{\left(CS\right)^2+2L_{14}L_{26}+\sqrt{\left(CS\right)^4+\left(2L_{14}L_{26}\right)^2+4\left(CS\right)^2L_{14}L_{26}+4\left(L_{14}L_{27}\right)^2}}\right]$$

$$L_{29}=\frac{1}{2L_{14}}\left[\sqrt{-\left(CS\right)^2-2L_{14}L_{26}+\sqrt{\left(CS\right)^4+\left(2L_{14}L_{26}\right)^2+4\left(CS\right)^2L_{14}L_{26}+4\left(L_{14}L_{27}\right)^2}}\right]$$

$$L_{30}=-EG_r \quad L_{31}=L_{14}L_8{}^2-L_{14}L_9{}^2-L_{12}SL_8-L_{26} \quad L_{32}=2L_{14}L_8L_9-L_{12}SL_9-L_{27}$$